HUNGARIAN AGRICULTURAL ENGINEERING
No 43/2024 5-17
Published online: http://hae-journals.org/
HU ISSN 0864-7410 (Print)
HU ISSN 2415-9751(Online)
DOI: 10.17676/HAE.2024.43.5
Received: 02.04.2024 - Accepted: 30.04.2024

PERIODICAL
OF THE COMMITTEE OF AGRICULTURAL AND BIOSYSTEM ENGINEERING OF THE HUNGARIAN ACADEMY OF SCIENCES
and
HUNGARIAN UNIVERSITY OF AGRICULTURE AND LIFE SCIENCES
INSTITUTE OF TECHNOLOGY

FINITE ELEMENT METHOD (CFX) INVESTIGATION OF THE FLUID FLOW DISTRIBUTION BEHAVIOR OF BOTH PARALLEL AND COUNTER TYPES OF HEAT EXCHANGERS

Author(s):
S. Hailemariam[1,2], J. Beke[1], I. Oldal[1], G. Kalácska[1]

Affiliation:
[1] Doctoral School of Mechanical Engineering – Hungarian University of Agriculture and Life Sciences, 2100 Gödöllő, Páter Károly u. 1., Hungary;
[2] Wollo University Kombolcha Institute of Technology School of Mechanical and Chemical Engineering Industrial Engineering Department, Wollo University, 1145 Dessie, Ethiopia

Email address:
shegawh@yahoo.com; beke.janos@uni-mate.hu; oldal.istvan@uni-mate.hu; kalacska.gabor@uni-mate.hu

Abstract: The thermal heat transfer behavior of hot and cold fluids within boundary conditions on both parallel and counter types of heat exchangers was investigated in this work using the computational fluid dynamics (CFD) approach in ANSYS Workbench (CFX). This technique helps us identify the precise values for the velocity, pressure, and temperature readings along and across the heat exchanger, in addition to determining how the three variables were distributed locally or globally. Cold water at 5 m/s and 20 °C, with a zero pressure at outlet or zero gauge pressure at outlet, was employed in this study, as was hot water at 4 m/s and 90 °C, with the zero pressure at outlet or zero gauge pressure at outlet. The results of any local or global temperature, pressure, and velocity values were represented along the length of both parallel and counter types of heat exchangers by color contours, where red indicated the largest value and blue the lowest. All of the global temperature, pressure, and velocity distributions were shown by charts positioned along the length of both parallel and counter-type heat exchangers. We came to the conclusion that when hot inlet fluid passes between the head and outer surface of cold fluid, there is a T-junction where high pressure and low velocity coexist. In comparison to parallel flow, the pressure and velocity distributions are lower in counter flow.

Keywords: ANYSY (CFX), CFD, heat transfer, pressure, temperature, thermal

1. Introduction

In many fields, efficient use of heat transfer is crucial, and because heat makes up a significant amount of final energy, it presents a significant barrier to the economic viability of many industrial processes [1–4]. The thermal engineering topic of study known as heat transfer is change, interchange, utilization, and formation of heat between bodies. Heat transport mechanisms include phase shift, conversion, radiation, and conduction. Heat exchangers are widely employed in industries [5–12]. Engineering applications in daily life and the industrial sector frequently use heat exchangers that are both parallel and counter [13–15]. Finding appropriate solutions is difficult since these heat exchangers are susceptible to thermal conduction, convection, radiation, and phase shifts in which energy is transmitted. To completely comprehend pressure distribution, temperature variation, and velocity variation in both parallel and counter-type heat exchangers from hot to cold is a significant phenomenon that necessitates substantial experimental investigation and numerical analysis. ANSYS CFX, a CFD modeling package, was used to evaluate the temperature variation and velocity on the flue, fin, and tube domains [16–18]. Complex phenomena such as thermal heat transfer between hot and cold fluids have been solved by modern technology. Researchers have used the commercial CFD code ANSYS to study the flue gas/water type parallel and counter heat exchangers [13–18]. Examining

the distribution and determine velocity, pressure, and velocity at any point within and across both parallel and counter types of heat exchangers is the goal of this work.

2. Materials and Methods

The distribution and calculation of pressure, temperature, velocity vector, streamlines, and velocity of both parallel and counter heat exchangers were all simulated with the use of the ANSYS Workbench software (CFX) and the computational fluid dynamics (CFD) method. Cold water was used at 5 m/s and 20 °C with the zero pressure at outlet or zero gauge pressure at outlet, while hot water was used at 4 m/s and 90 °C with zero pressure at outlet or zero gauge pressure at outlet. Fig. 1 depicts the steps of performing a general ANSYS workbench (CFX) and computational fluid dynamics while performing thermal heat transfer.

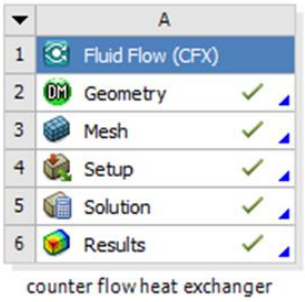

Figure 1. Steps in ANSYS CFX.

Assembly drawings generated by ANSYS Workbench Design Modular, along with the components for the hot and cold fluids within a 50-mm-diameter and 50-mm-high hot fluid cylinder in two different configurations, were used in the study. The dimensions of the hot fluid were two heads separated by 50 mm, and the cold fluid was 1000 mm long and 100 mm wide.

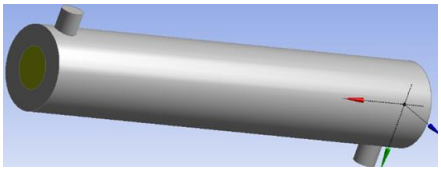

Figure 2. 3D model of cold fluid and hot fluid.

Numerous researchers employed loads and boundary conditions while using CFD and the FEM to simulate the characteristics of heat exchanger [9], and [19–32]. As seen in Fig. 3, giving names to both parallel fluid flow and counter fluid flow bodies cold fluid and their surfaces like cold fluid in face represented by letter A, cold fluid out face denoted by letter B, cold wall denoted by letter C and cold domain denoted by letter D.

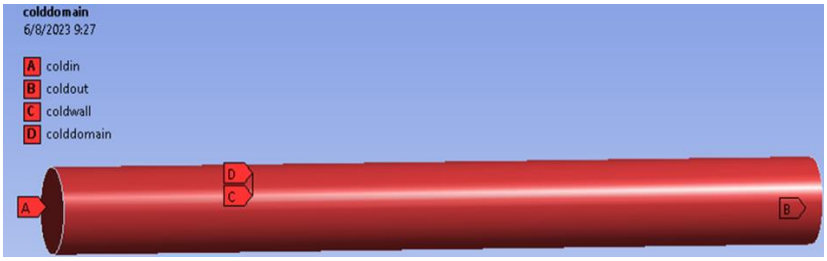

Figure 3. The naming of cold fluid.

As seen in Fig. 4, giving names to both parallel fluid flow and counter fluid flow bodies hot fluid and their surfaces like hot out fluid in face represented by letter A, hot fluid in face denoted by letter B, hot inner wall

denoted by letter C, hot outer walls denoted by letter D, hot faces represented by letter E and hot domain represented by letter F.

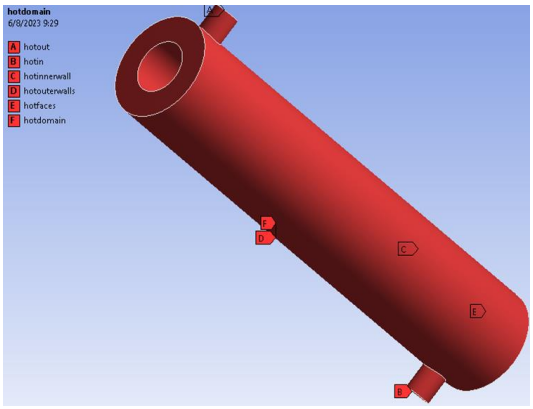

Figure 4. The naming of hot fluid.

The next stage in this research was to create contacts between the surfaces of the hot and cold fluids by connecting them. Fig. 5 in the below illustration illustrates how to create hot and cold fluid contact surfaces in the ANSYS workbench. As Fig. 5 makes evident, the target body is indicated by the blue colour, and the contact region is indicated by the red colour. You can also flip the setting.

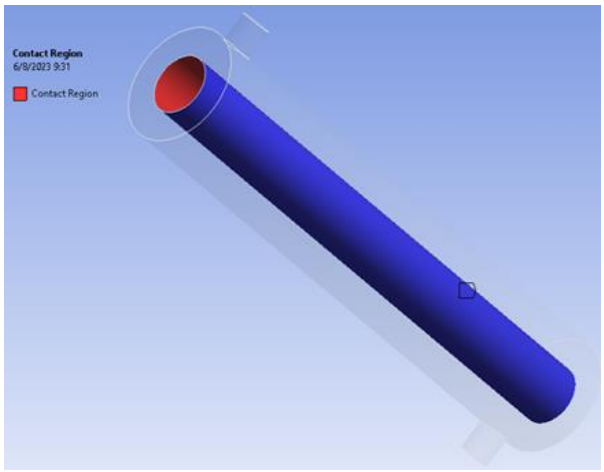

(a) Contact region and target body

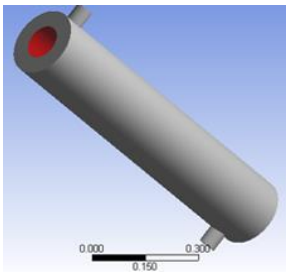

(b) Contact region

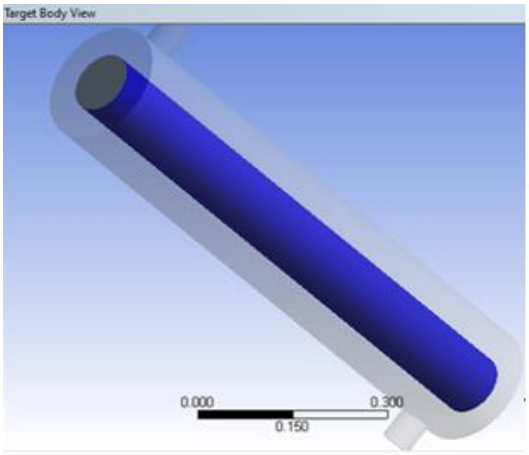

(c) Target body

Figure 5. Contact surfaces of cold fluid and hot fluid.

ANSYS geometry was used to define the computational fluid domain (CFD) was utilized to discretize the domain [33–39]. The discretization of the fluid model into a "mesh" composed of multiple elements is an essential precondition for the ANSYS CFX and CFD methodologies. The mesh size is influenced by numerous factors in the fluid model, such as density windows, surface curvatures, spacing between geometric entities, and field variable distribution [11], [12], [19], [22], [26] and [27]. The steps of inflation on the circumferential sides and the size of all edges are utilized as shown in Fig. 6.

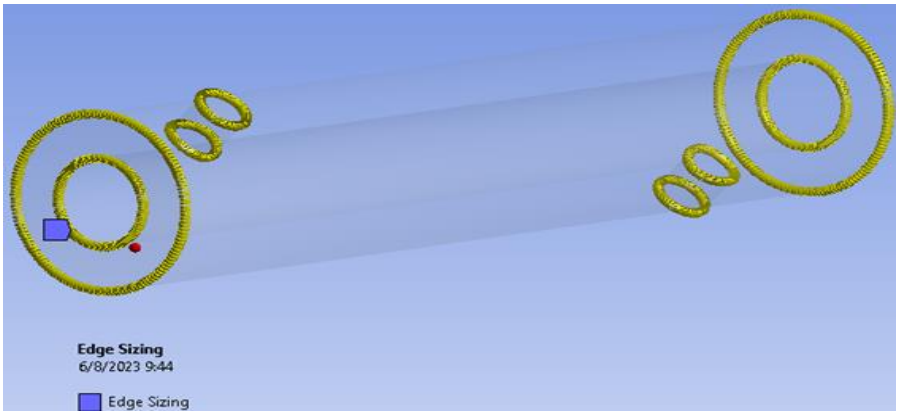

Figure 6. Edge meshing by division of numbers.

In three-dimensional numerical analysis, tetrahedrons, hexahedrons, and their combinations are commonly utilized. Highly efficient, easily implemented, flexible for creating adaptive meshes, and easily re-generable meshes are the advantages of tetrahedral element meshes. The automatic generation technology of tetrahedral element meshes is currently fully developed and finds widespread application in handling complex geometry. As demonstrated in Fig. 7, adaptive generation for the use and refining of tetrahedral meshes was also utilised in this work.

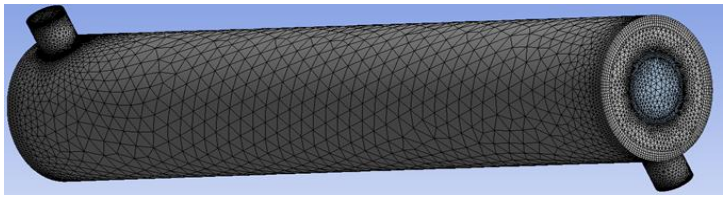

Figure 7. A mesh model of hot fluid and cold fluid.

Setup: Select water from the material library in this step. The fluid model was thermal energy. In the first case of parallel fluid flow, the hot and cold fluid assemblies would be subjected to all boundary conditions. Cold water was applied at the inlet at 5 m/s and 20 °C with zero length of cold fluid, and cold water was applied at the outlet at zero pressure and zero length of cold fluid. Furthermore, hot water was applied at the inlet at 4 m/s and 90 °C, 50 mm away from the edge of the hot fluid on the head, at 4 m/s and 90 °C.

Figure 8. Setup boundaries for parallel fluid flow.

The assemblies would then be subjected to all boundary conditions in the second case in a counter-fluid flow. Cold water was applied at the inlet at a 5 m/s and at a 20 °C with zero length of cold fluid, and zero pressure of cold water was applied at the outlet or end length of cold fluid. And also, hot water was applied at the input 4 m/s and 90 °C at 50 mm away from the edge of the hot fluid on the head on another side (950

mm away from the origin of the hot fluid) and at zero pressure of hot water at 50 mm away from the edge of the hot fluid flow on the heads. In addition, these applied wall boundary conditions to the two faces and the three outer sides of the hot fluid. Furthermore, the interface boundary between the cold outer face and the hot inner face was applied for heat transfer.

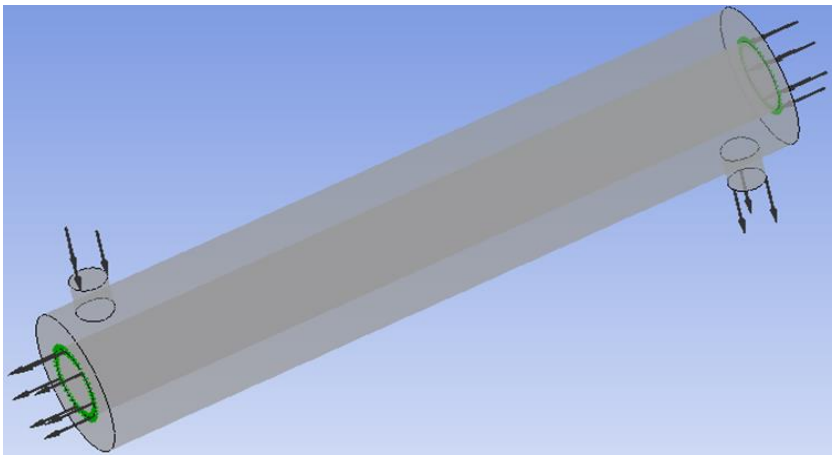

Figure 9. Setup of counter fluid flow.

3. Results

The simulation results below show the overall outcomes of both the parallel fluid flow and the counter-fluid flow, including streamlines of velocities, pressure distribution contours, pressure distribution charts, global velocity distribution contour plots, velocity vector distribution, global temperature distribution contour plots, and temperature distribution layouts. Fig. 10 shows below the streamline of velocities both (a) parallel fluid flow and (b) counter fluid flow using both inlets and outlets of cold and hot fluid flow; the red represents the maximum, and the blue denotes the minimum.

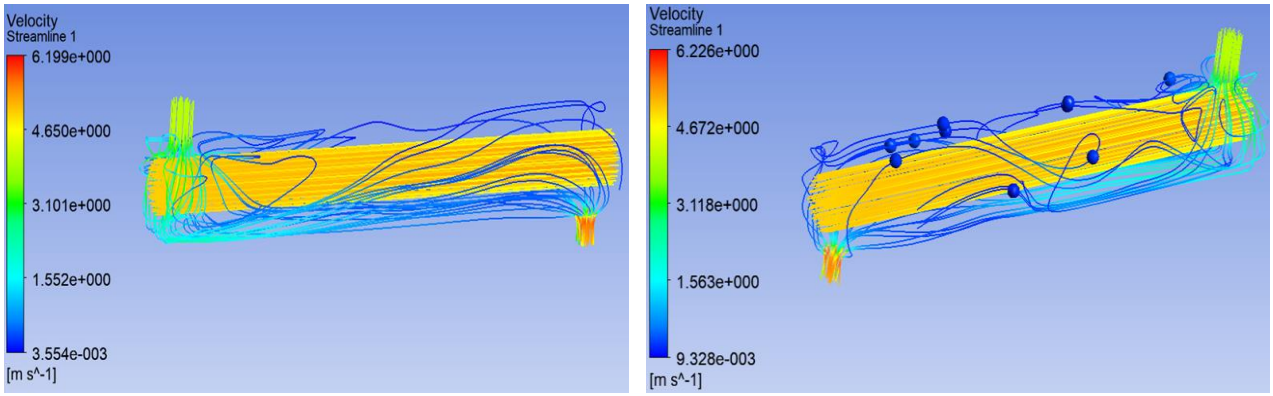

(a) Parallel fluid flow *(b)* Counter fluid flow

Figure 10. Shows streamlines of velocities.

Fig. 11 shows below the contour of the pressure distribution (global) of (a) parallel fluid flow and (b) counter fluid flow; the red shows high pressure and the blue represents low pressure. A T-junction is formed 50 mm away from the origin of the shell and tube when hot incoming fluid passes between the head and surface of the cool fluid as shown in Fig. 11 (a) parallel fluid flow. High pressure and low velocity coexist here. When hot inlet fluid flows through the head and makes contact with the cool fluid's contact surface, a T-junction forms 950 mm from the origin at the cold fluid's edge as shown in Fig. 11 (b) counter fluid flow. In this area, high pressure and low velocity coexist.

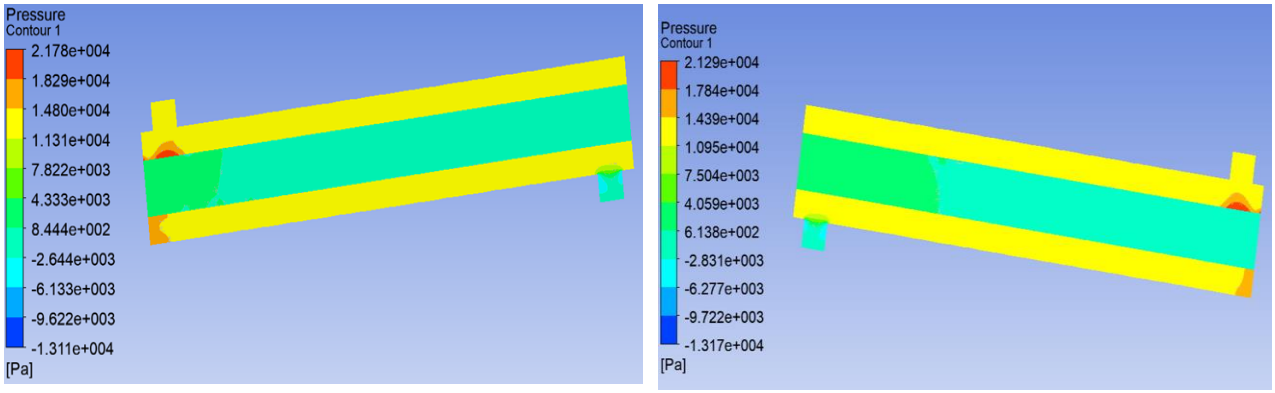

(a) Parallel fluid flow *(b)* Counter fluid flow

Figure 11. The contour of pressure distribution.

The pressure distribution charts for (a) parallel fluid flow and (b) counter fluid flow are displayed below in Fig. 12a and Fig. 12b. A chart of the pressure distribution (global) collected from 150 streamlines. Both the length and the pressure distribution are shown by the x and y axes, respectively. In case of (a) parallel fluid flow, when hot inlet fluid flows pass through the head and make contact with the cool fluid's contact surface, a T-junction forms 50 mm from the origin at the cold fluid's edge. In this region, high pressure and low velocity coexist. A T-junction is formed when hot fluid passes through the head and separates the surface of the cool fluid, 950 mm away from the origin of the cold fluid. In this region, low pressure and high velocity coexist. The reverse is true in case of (b) counter fluid flow case.

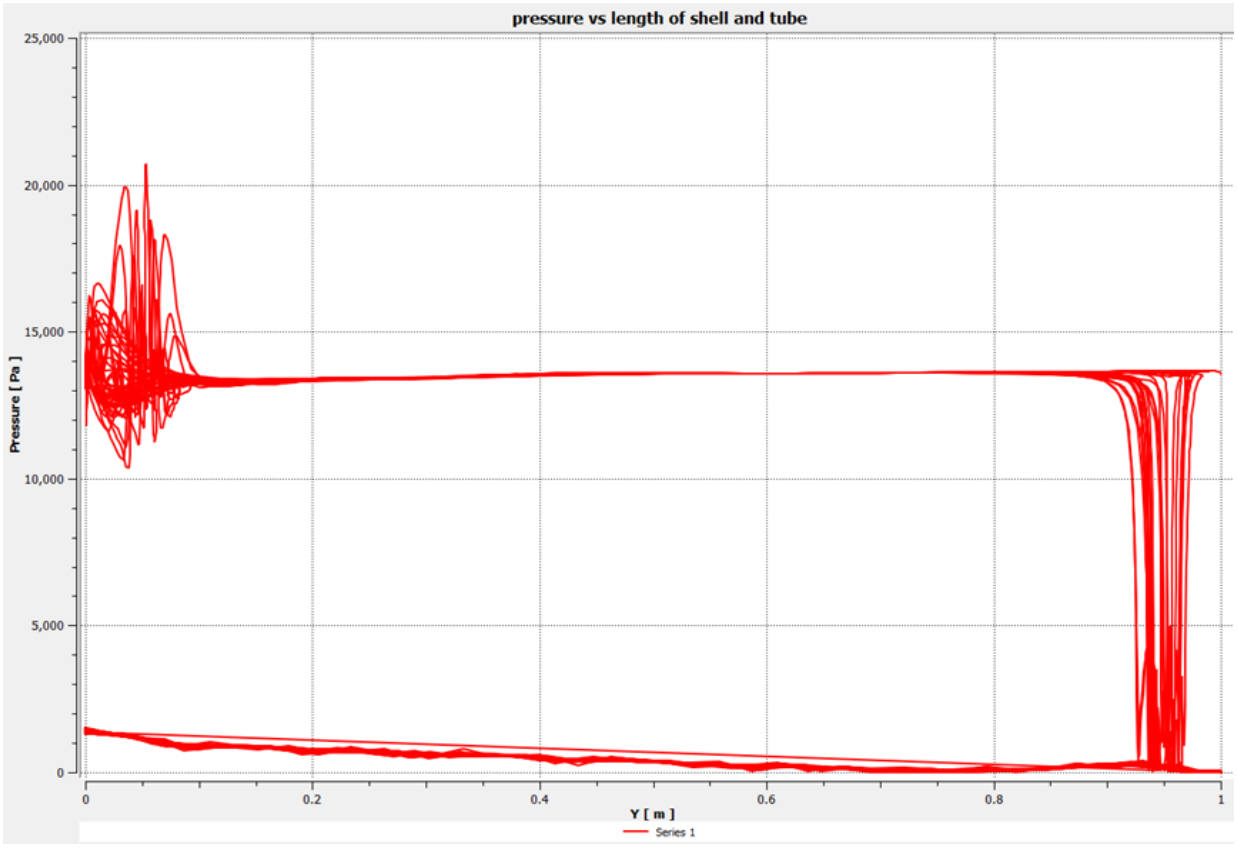

(a) Parallel fluid flow

Figure 12a. Pressure distribution graphs.

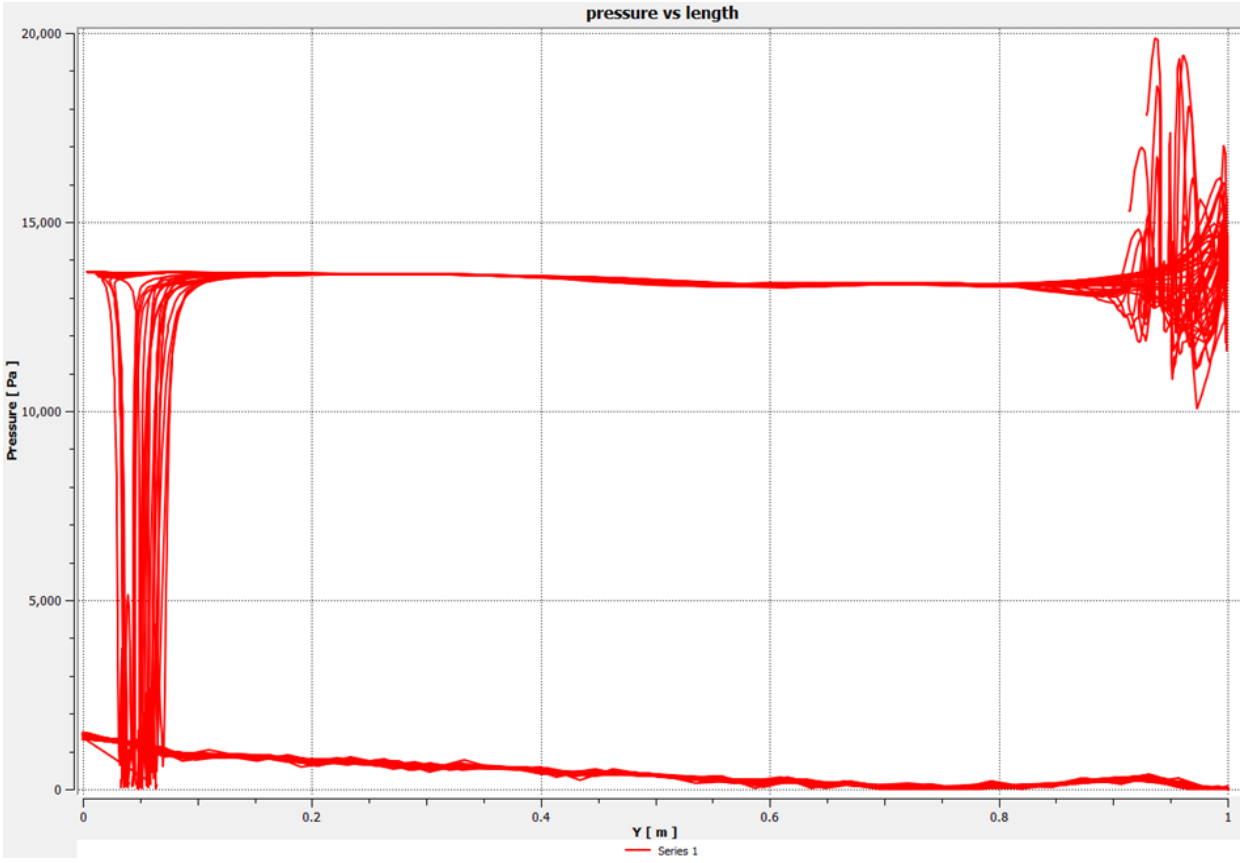

(b) Counter-fluid flow

Figure 12b. Pressure distribution graphs.

Fig. 13 shows the global velocity variation in both (a) parallel fluid flow and (b) counter fluid flow in the contour plot. The maximum velocity is shown in red, while the minimum velocity is shown in blue. In the pressure distribution charts for (a) parallel fluid flow and (b) counter fluid flow, as we elaborated before, the opposite is true. This implies that a certain region will have low velocity values when high pressure values occur.

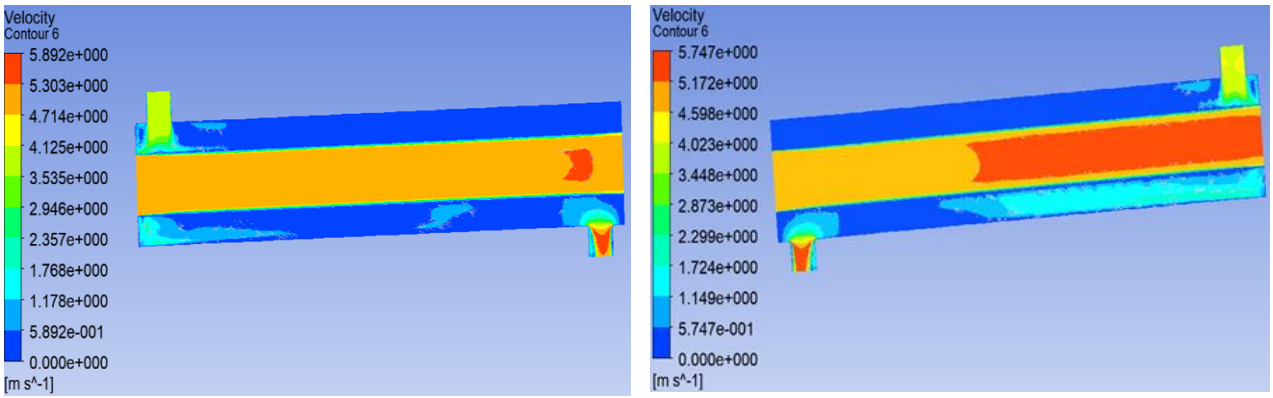

(a) Parallel fluid flow *(b)* Counter fluid flow

Figure 13. Global velocity distribution contour plot.

The velocity vector distribution for both (a) parallel fluid flow and (b) counter fluid flow is depicted below in Fig. 14. The highest velocity of the vector is denoted by the red arrow, while its minimum velocity is given by the blue arrow.

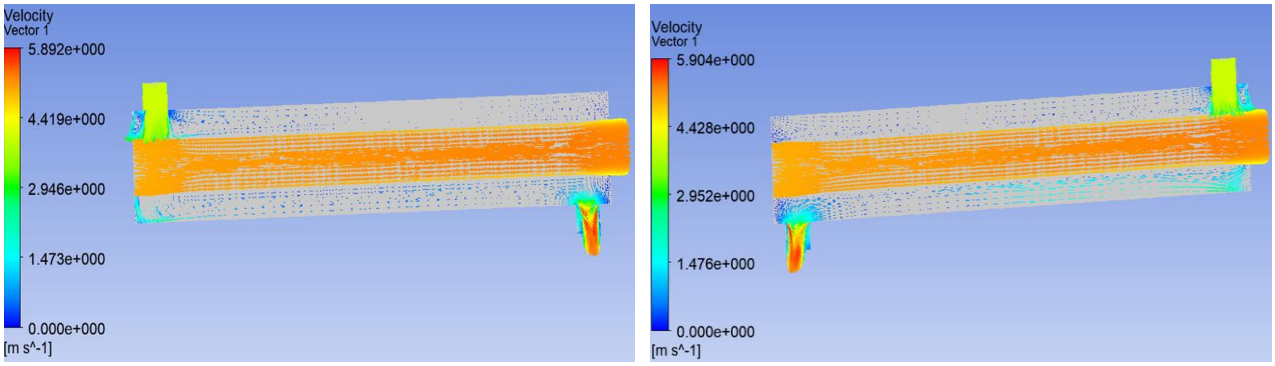

(a) Parallel fluid flow *(b)* Counter fluid flow

Figure 14. Velocity vector distribution.

Below are velocity distribution charts for (a) parallel fluid flow and (b) counter fluid flow, as shown in Fig. 15a and Fig. 15b. This represents the velocity variation on the y-axis and lengths on the x-axis. The chart of velocity distribution (global) obtained from the collection of 150 streamlines' dates. In (b) counter fluid flow Fig 15b, when hot inlet fluid flows through the head and makes contact with the cool fluid's contact surface, a T-junction forms 950 mm from the origin at the cold fluid's edge. In this area, high pressure and low velocity coexist. However, a T-junction is formed when hot fluid passes through the head and separates the surface of the cool fluid 50 mm away from the origin of the cold fluid. This region has both low pressure and high velocity. The reverse is true in case of (a) parallel fluid flow case. (Fig. 15a)

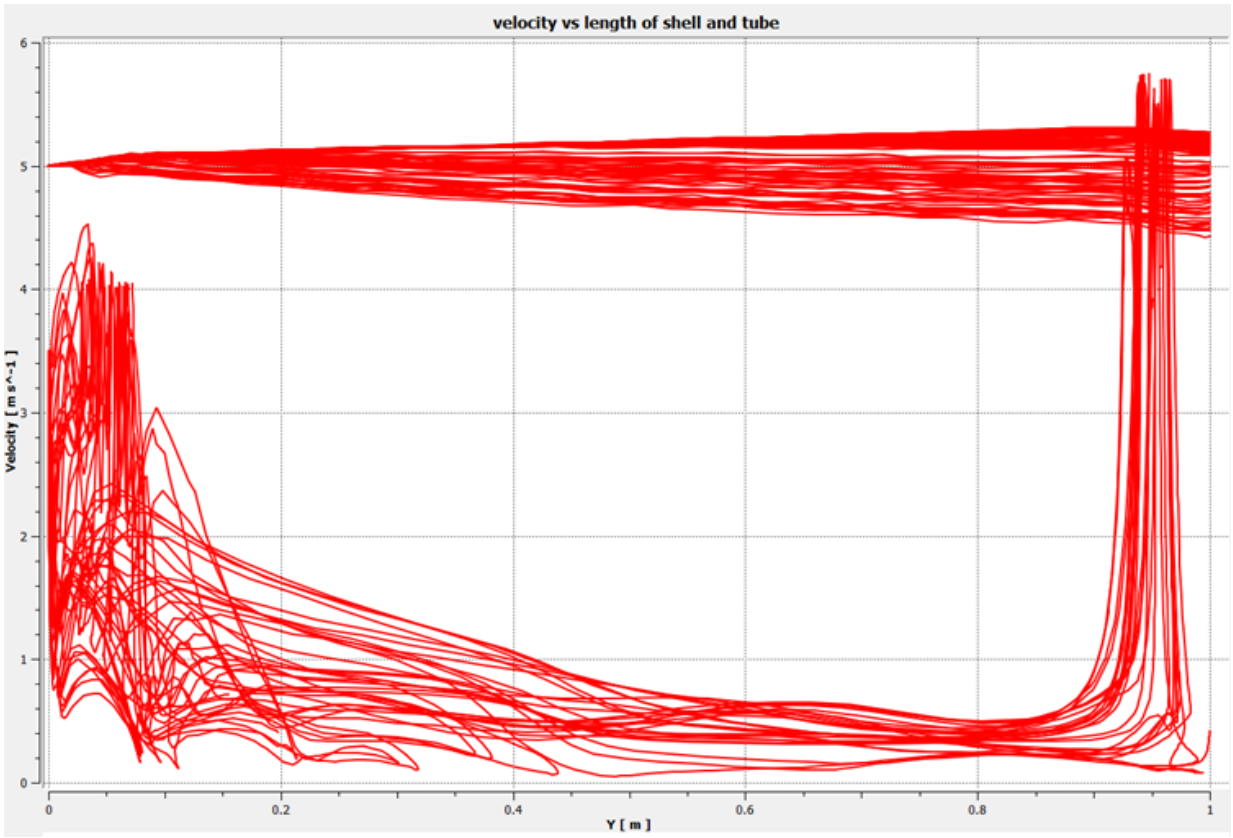

(a) Parallel fluid flow

Figure 15a. Velocity distribution graphs.

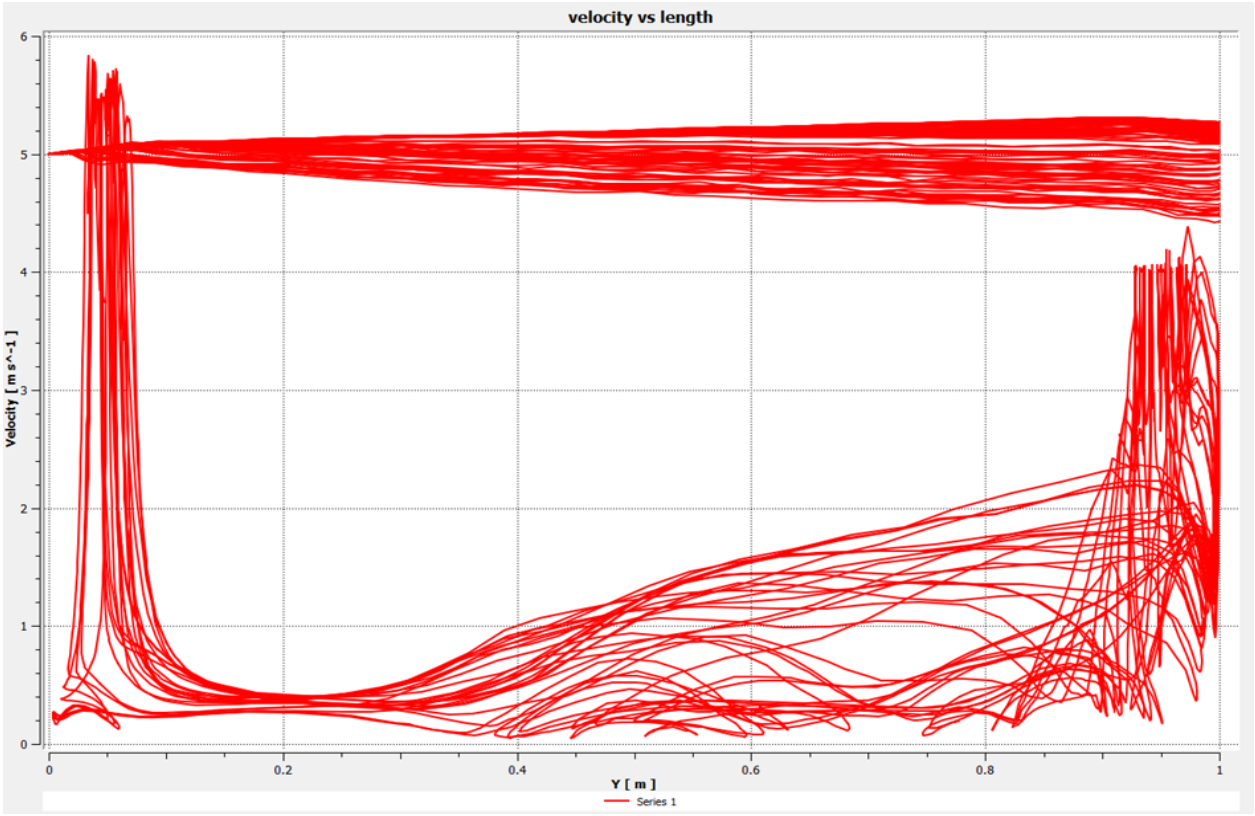

(b) Counter fluid flow

Figure 15b. Velocity distribution graphs.

The contour plots below represent the global temperature distribution for both (a) parallel fluid flow and (b) counter fluid flow, as seen in Fig. 16. The highest temperature is displayed by the red and the lowest is indicated by the blue. From the through head's intake to the out-through head on another, the heated fluid is continuously dripping out for either parallel fluid flow or counter fluid flow as show below temperature contour plots.

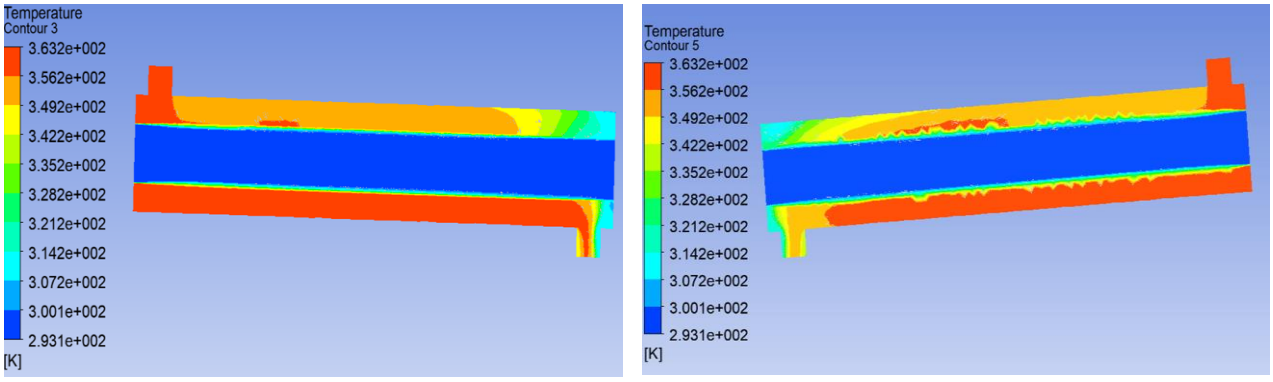

(a) Parallel fluid flow *(b)* Counter fluid flow

Figure 16. Global temperature distribution contour plots.

The temperature distribution charts for (a) parallel fluid flow and (b) counter fluid flow are displayed in Fig. 17 below. The chart of the temperature distribution (global) from 150 streamline collection dates. The temperature distribution is denoted by the y-axis, while the length is denoted by the x-axis. Temperature staring, dropping the hot fluid inlet through the head, and contact with cold fluid form a T-junction that is 50 mm away from the edge of cold fluid up to 950 mm away from the origin coordinate of cold fluid to hot fluid out, as shown in this temperature distribution chart in case of (a) parallel fluid flow in Fig. 17. From the

head's 950 mm T-junction, where the hot fluid begins to continually decrease in temperature, the cold fluid continues to do so until it reaches the head's hot flow outlet, which is located 50 mm from the cold fluid's source for the case of (b) counter fluid flow in Fig. 17.

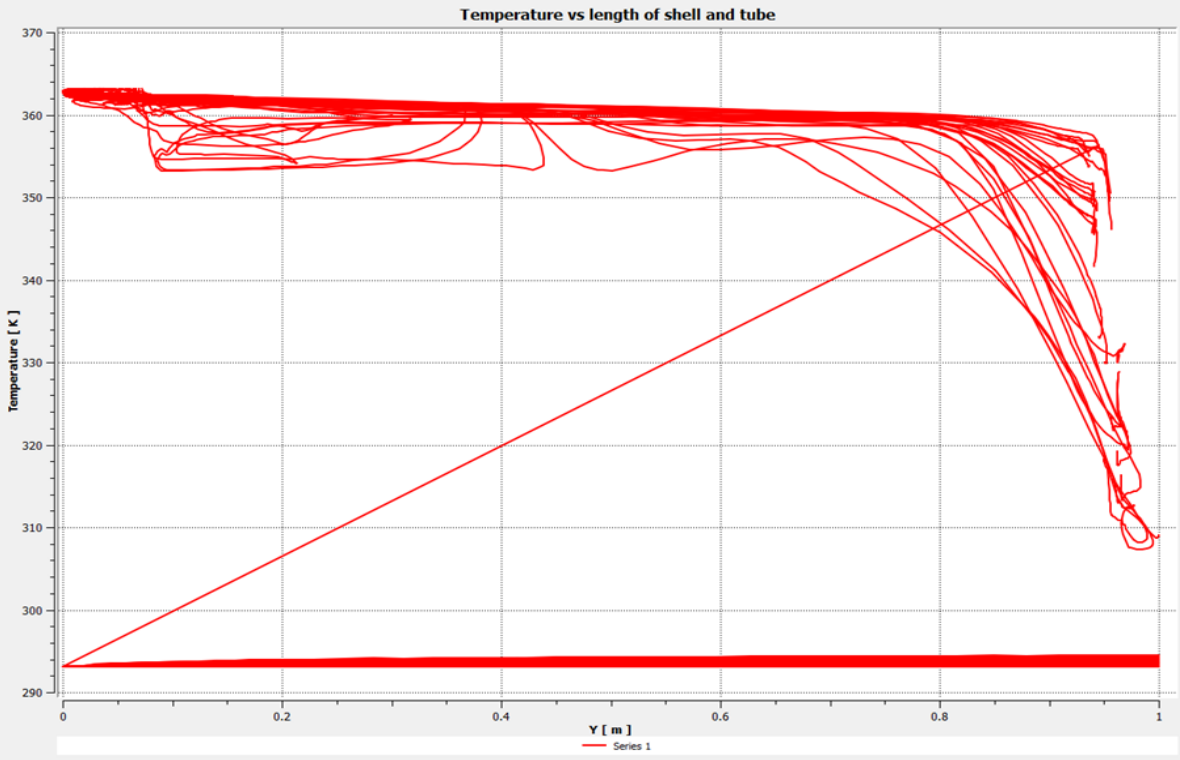

(a) Parallel fluid flow

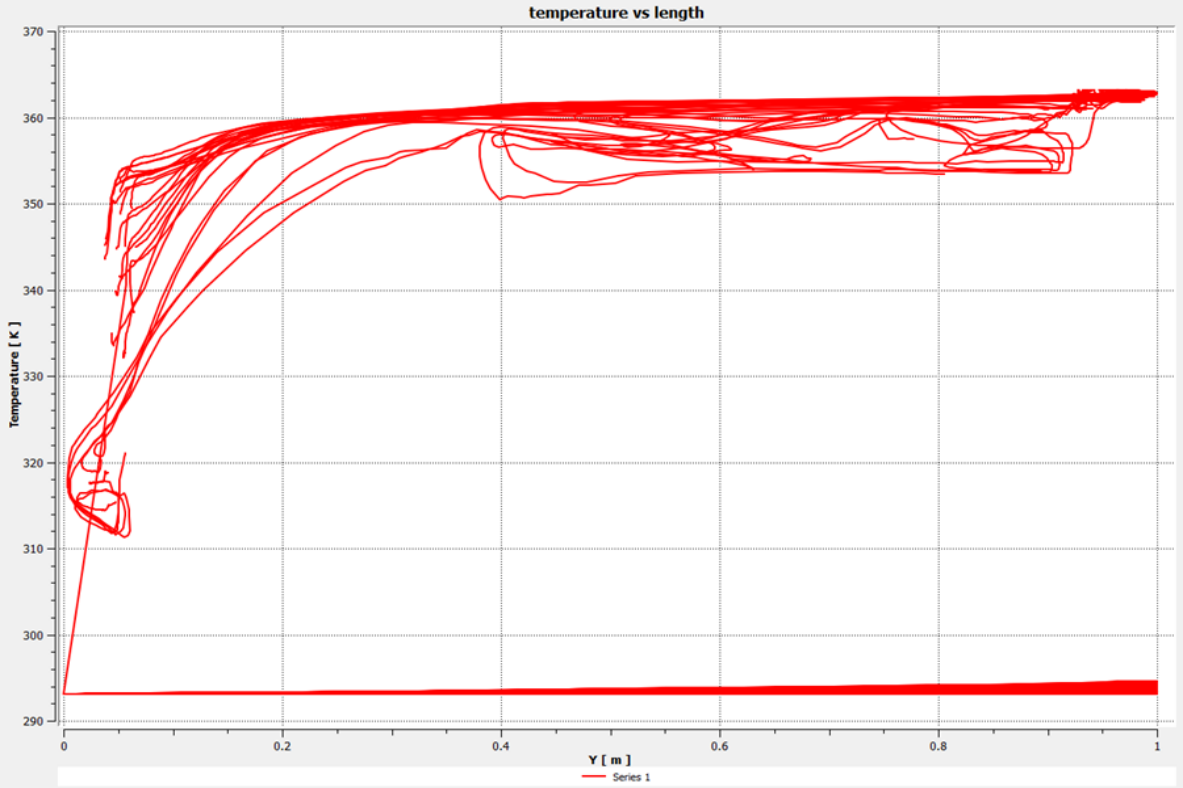

(b) Counter fluid flow

Figure 17. Temperature distribution plots.

4. Discussion

The overall results show that the parameters of pressure, temperature, and velocity do not significantly alter between parallel and counter fluid flow. The researchers demonstrated fluid flow animation using a velocity stream [11], [19], [31], [32], [37], [40], and [41]. The fluid flow character and pressure distribution approaching the T junction are complicated due to the sudden widening of the flow boundary, which results in flow separation and variable distribution [9], and [31]. The pressure is maximum at the end of the header and minimum at the entrance due to the jet caused at the inlet [27], [42], and [43]. In light of this, our findings were consistent with the study. Along the header inlet, the velocity is high, a clear vortex is circulated along the sides of the expanded jet flow, and a minor eddy flow is seen close to the header inlet because the vortex flow's circulation would slow down the first velocity [3], [27], [29], [37], [38], [39], and [42]. When the flow is flowing downstream, the turbulent kinetic energy and dissipation rate are greatest close to the T junction; they gradually decrease as the flow proceeds downstream, and they completely vanish near the closed end of the manifold [9]. As a result, our findings are consistent with those of other researchers. Researches demonstrated using velocity vectors [3], [9], [12], [16], [24], [25], [35], [37], [40] and [41]. Temperature measurements revealed a decrease in flow direction [6], [12], [20], [21], [22], [23] and [32]. A similar result occurs when hot fluid constantly transfers heat to cold fluid and hot fluid gradually decreases throughout the length, as shown in Fig. 17 global temperature distribution contour.

5. Conclusions

Fluid flows in the heat exchanger were analyzed using ANSYS Workbench CFX computational fluid dynamics, both parallel and counter types of heat exchangers. A detailed discussion was held regarding the temperature, pressure, and temperature throughout the entire heat exchanger. Here is a summary of the findings: The overall flow rate increases when the pressure differential decreases. High pressure and low velocity coexist at a T-junction, which is created when hot inlet fluid passes through the head and outer surface of cold fluid. Compared to parallel flow, counter flow has lower pressure and velocity distributions. Both parallel and counter types of heat exchangers can be successfully analyzed in all velocity distribution, pressure distribution, and temperature distribution using the ANSYS workbench (CFX) and computational fluid dynamics approach.

References

[1] **Zambaux, J. A., Harion, J. L., Russeil, S., & Bouvier, P.**, (2015). The effect of successive alternating wall deformation on the performance of an annular heat exchanger. Applied Thermal Engineering, 90, 286-295.

[2] **Sajadi, A. R., Sorkhabi, S. Y. D., Ashtiani, D., & Kowsari, F.**, (2014). Experimental and numerical study on heat transfer and flow resistance of oil flow in alternating elliptical axis tubes. International Journal of Heat and Mass Transfer, 77, 124-130.

[3] **Han, H. Z., Li, B. X., Wu, H., & Shao, W.**, (2015). Multi-objective shape optimization of double pipe heat exchanger with inner corrugated tube using RSM method. International Journal of Thermal Sciences, 90, 173-186.

[4] **Omidi, M., Farhadi, M., & Jafari, M.**, (2017). A comprehensive review on double pipe heat exchangers. Applied Thermal Engineering, 110, 1075-1090.

[5] **Yang, M., Low, E., Law, C. L., Chen, J. C., Show, P. L., & Huang, S. M.**, (2022). Heat and mass transfer in a counter flow parallel plate membrane-based absorption heat pump (PMAHP). International Journal of Thermal Sciences, 171, 107227.

[6] **Sheikholeslami, M., Hatami, M., Jafaryar, M., Farkhadnia, F., Ganji, D. D., & Gorji-Bandpy, M.**, (2015). Thermal management of double-pipe air to water heat exchanger. Energy and Buildings, 88, 361-366.

[7] **Yehia, M. G., Attia, A. A., Abdelatif, O. E., & Khalil, E. E.**, (2016). Heat transfer and friction characteristics of shell and tube heat exchanger with multi inserted swirl vanes. Applied Thermal Engineering, 102, 1481-1491.

[8] **Tavousi, E., Perera, N., Flynn, D., & Hasan, R.**, (2023). Heat transfer and fluid flow characteristics of the passive method in double tube heat exchangers: a critical review. International Journal of Thermofluids, 17, 100282.

[9] **Minocha, N., & Joshi, J. B.**, (2020). 3D CFD simulation of turbulent flow distribution and pressure drop in a dividing manifold system using openfoam. International Journal of Heat and Mass Transfer, 151, 119420.

[10] **Andhare, R. S., Shooshtari, A., Dessiatoun, S. V., & Ohadi, M. M.**, (2016). Heat transfer and pressure drop characteristics of a flat plate manifold microchannel heat exchanger in counter flow configuration. Applied Thermal Engineering, 96, 178-189.

[11] **Ozden, E., & Tari, I.**, (2010). Shell side CFD analysis of a small shell-and-tube heat exchanger. Energy conversion and Management, 51(5), 1004-1014.

[12] **Liu, J. J., Liu, Z. C., & Liu, W.**, (2015). 3D numerical study on shell side heat transfer and flow characteristics of rod-baffle heat exchangers with spirally corrugated tubes. International journal of thermal sciences, 89, 34-42.

[13] **Zhou, J., Sun, Z., Ding, M., Bian, H., Zhang, N., & Meng, Z.**, (2017). CFD simulation for flow distribution in manifolds of central-type compact parallel flow heat exchangers. Applied Thermal Engineering, 126, 670-677.

[14] **Yaïci, W., Ghorab, M., & Entchev, E.**, (2013). Numerical analysis of heat and energy recovery ventilators performance based on CFD for detailed design. Applied Thermal Engineering, 51(1-2), 770-780.

[15] **Huang, S. M., Yang, M., Huang, W. H., Tao, S., Hu, B., & Qin, F. G.**, (2018). An analytical solution of heat and mass transfer in a counter/parallel flow plate membrane module used in an absorption heat pump. International Journal of Thermal Sciences, 124, 110-121.

[16] **Gorman, J. M., Krautbauer, K. R., & Sparrow, E. M.**, (2016). Thermal and fluid flow first-principles numerical design of an enhanced double pipe heat exchanger. Applied Thermal Engineering, 107, 194-206.

[17] **Łopata, S., & Ocłoń, P.**, (2015). Numerical study of the effect of fouling on local heat transfer conditions in a high-temperature fin-and-tube heat exchanger. Energy, 92, 100-116.

[18] **Taler, D., & Ocłoń, P.**, (2014). Thermal contact resistance in plate fin-and-tube heat exchangers, determined by experimental data and CFD simulations. International Journal of Thermal Sciences, 84, 309-322.

[19] **Hari, B., Brouwer, J. P., Dhir, A., & Steinberger-Wilckens, R.**, (2019). A computational fluid dynamics and finite element analysis design of a microtubular solid oxide fuel cell stack for fixed wing mini unmanned aerial vehicles. International Journal of Hydrogen Energy, 44(16), 8519-8532.

[20] **Modi, N., Wang, X., Negnevitsky, M., & Cao, F.**, (2021). Melting characteristics of a longitudinally finned-tube horizontal latent heat thermal energy storage system. Solar Energy, 230, 333-344.

[21] **Hatami, M., Jafaryar, M., Ganji, D. D., & Gorji-Bandpy, M.**, (2014). Optimization of finned-tube heat exchangers for diesel exhaust waste heat recovery using CFD and CCD techniques. International Communications in Heat and Mass Transfer, 57, 254-263.

[22] **Kumar, P. M., & Chandrasekar, M.**, (2019). CFD analysis on heat and flow characteristics of double helically coiled tube heat exchanger handling MWCNT/water nanofluids. Heliyon, 5(7).

[23] **Zhou, F., Ling, W., Zhou, W., Qiu, Q., & Chu, X.**, (2019). Heat transfer characteristics of Cu-based microchannel heat exchanger fabricated by multi-blade milling process. International Journal of Thermal Sciences, 138, 559-575.

[24] **Gandhi, M. S., Ganguli, A. A., Joshi, J. B., & Vijayan, P. K.**, (2012). CFD simulation for steam distribution in header and tube assemblies. Chemical Engineering Research and Design, 90(4), 487-506.

[25] **Tamburini, A., Renda, M., Cipollina, A., Micale, G., & Ciofalo, M.**, (2016). Investigation of heat transfer in spacer-filled channels by experiments and direct numerical simulations. International Journal of Heat and Mass Transfer, 93, 1190-1205.

[26] **Su, L., Duan, Z., He, B., Ma, H., & Ding, G.**, (2019). Laminar flow and heat transfer in the entrance region of elliptical minichannels. International Journal of Heat and Mass Transfer, 145, 118717.

[27] **Cupiał, P., & Snamina, J.**, (2022). Analytical and numerical approach to convective heat transfer through a granular target with gas cooling. International Journal of Thermal Sciences, 171, 107196.

[28] **Yang, H., Wang, Y., Ren, M., & Yang, X.**, (2017). Effect of the rectangular exit-port geometry of a distribution manifold on the flow performance. Applied Thermal Engineering, 117, 481-486.
[29] **Jayakumar, J. S., Mahajani, S. M., Mandal, J. C., Vijayan, P. K., & Bhoi, R.**, (2008). Experimental and CFD estimation of heat transfer in helically coiled heat exchangers. Chemical engineering research and design, 86(3), 221-232.
[30] **Hashemian, M., Jafarmadar, S., & Dizaji, H. S.**, (2016). A comprehensive numerical study on multi-criteria design analyses in a novel form (conical) of double pipe heat exchanger. Applied thermal engineering, 102, 1228-1237.
[31] **Zhang, W., Li, A., Gao, R., & Li, C.**, (2018). Effects of geometric structures on flow uniformity and pressure drop in dividing manifold systems with parallel pipe arrays. International Journal of Heat and Mass Transfer, 127, 870-881.
[32] **Bezaatpour, M., & Goharkhah, M.**, (2020). Convective heat transfer enhancement in a double pipe mini heat exchanger by magnetic field induced swirling flow. Applied Thermal Engineering, 167, 114801.
[33] **Hashemian, M., Jafarmadar, S., Nasiri, J., & Dizaji, H. S.**, (2017). Enhancement of heat transfer rate with structural modification of double pipe heat exchanger by changing cylindrical form of tubes into conical form. Applied Thermal Engineering, 118, 408-417.
[34] **Li, B., Hou, J., Xu, K., Gao, Q., Zeng, M., & Wang, Q.**, (2023). Optimal designs for flow uniformity at inlet of microchannel flat tube heat exchanger. Applied Thermal Engineering, 226, 120300.
[35] **Sen, N., Tat, D., Singh, K. K., Goswami, A. K., Mukhopadhyay, S., & Shenoy, K. T.**, (2022). Single-phase flow distribution and mixing in a novel microfluidic header: Experimental and CFD studies. Chemical Engineering Research and Design, 188, 433-446.
[36] **Kirincic, M., Trp, A., & Lenic, K.**, (2021). Numerical evaluation of the latent heat thermal energy storage performance enhancement by installing longitudinal fins. Journal of energy storage, 42, 103085.
[37] **Raul, A., Bhasme, B. N., & Maurya, R. S.**, (2016). A numerical investigation of fluid flow maldistribution in inlet header configuration of plate fin heat exchanger. Energy Procedia, 90, 267-275.
[38] **Shojaeefard, M. H., Nourbakhsh, S. D., & Zare, J.**, (2017). An investigation of the effects of geometry design on refrigerant flow mal-distribution in parallel flow condenser using a hybrid method of finite element approach and CFD simulation. Applied Thermal Engineering, 112, 431-449.
[39] **Said, S. A. M., Ben-Mansour, R., Habib, M. A., & Siddiqui, M. U.**, (2015). Reducing the flow mal-distribution in a heat exchanger. Computers & Fluids, 107, 1-10.
[40] **Vali, A., Ge, G., Besant, R. W., & Simonson, C. J.**, (2015). Numerical modeling of fluid flow and coupled heat and mass transfer in a counter-cross-flow parallel-plate liquid-to-air membrane energy exchanger. International Journal of Heat and Mass Transfer, 89, 1258-1276.
[41] **Liu, H. L., Li, H., He, Y. L., & Chen, Z. T.**, (2018). Heat transfer and flow characteristics in a circular tube fitted with rectangular winglet vortex generators. International Journal of Heat and Mass Transfer, 126, 989-1006.
[42] **Wang, C. C., Yang, K. S., Tsai, J. S., & Chen, Y.**, (2011). Characteristics of flow distribution in compact parallel flow heat exchangers, part I: Typical inlet header. Applied Thermal Engineering, 31(16), 3226-3234.
[43] **Barrios, A. N. S., Silva, J. B. C., Rodrigues, A. R., Coelho, R. T., Junior, A. B., & Matsumoto, H.**, (2014). Modeling heat transfer in die milling. Applied thermal engineering, 64(1-2), 108-116.